HHS Public Access

Author manuscript

Cell Microbiol. Author manuscript; available in PMC 2018 July 01.

Published in final edited form as:

Cell Microbiol. 2017 July ; 19(7): . doi:10.1111/cmi.12728.

Helicobacter hepaticus cytolethal distending toxin promotes intestinal carcinogenesis in 129Rag2-deficient Mice

Zhongming Ge, **Yan Feng**, **Lili Ge**, **Nicole Parry**, **Suresh Muthupalani**, and **James G. Fox**

Division of Comparative Medicine, Massachusetts Institute of Technology, 77 Massachusetts Avenue, Cambridge, MA02139, U. S. A

Summary

Multiple pathogenic Gram-negative bacteria produce the cytolethal distending toxin (CDT) with activity of DNase I; CDT can induce DNA double strand breaks (DSBs), G2/M cell cycle arrest and apoptosis in cultured mammalian cells. However, the link of CDT to *in vivo* tumorigenesis is not fully understood. In this study, 129/SvEv *Rag2*$^{-/-}$ mice were gavaged with wild-type *Helicobacter hepatics* 3B1(Hh) and its isogenic *cdtB* mutant HhcdtBm7, followed by infection for 10 and 20 weeks (WPI). HhCDT-deficiency did not affect cecal colonization levels of HhcdtBm7, but attenuated severity of cecal pathology in HhcdtBm7-infected mice. Of importance, preneoplasic dysplasia was progressed to cancer from 10 WPI to 20 WPI in the Hh-infected mice but not in the HhcdtBm7-infected mice. In addition, the loss of HhCDT significantly dampened transcriptional upregulation of cecal *Tnfα* and *Il-6,* but elevated *Il-10* mRNA levels when compared to Hh at 10 WPI. Furthermore, the presence of HhCDT increased numbers of lower bowel intestinal γH2AX-positive epithelial cells (a marker of DSBs) at both 10 WPI and 20 WPI, and augmented phospho-Stat3 foci^{+} intestinal crypts (activation of Stat3) at 20 WPI. Our findings suggest that CDT promoted Hh carcinogenesis by enhancing DSBs and activation of the *Tnfα* / Il-6-Stat3 signaling pathway.

Introduction

Genomic instability is one of the most prominent characteristics in cancer cells (Hanahan & Weinberg, 2011). DNA damage such as double strands breaks (DSBs) and single strand breaks (SSBs), if left unrepaired or incorrectly repaired, can result in genomic mutations and structural rearrangement of the genome, which potentially leads to genomic stability (Lord & Ashworth, 2012). DNA damage can be induced by a wide variety of endogenous and exogenous agents, including ionizing radiation, oxidative free radicals, cigarette smoking, mutagenic chemicals present in environment and drugs used in chemotherapy (Lord & Ashworth, 2012; Helleday*, et al*., 2014). In addition, a group of pathogenic gram-negative bacteria including *Escherichia coli*, *Campylobacter* species, *Shigella dysenteriae*, *Haemophilus ducreyi*, select enterohepatic *Helicobacter* species, *Aggregatibacter* (formerly *Actinobacillus*) *actinomycetemcomitans, Providencia alcalifaciens,* and *Salmonella enterica* serovar Typhi produce a genotoxin, namely cytolethal distending toxins (CDTs) (Guerra*, et*

Correspondence to Zhongming Ge, zge@mit.edu; Phone: (617) 253-5518; Fax: (617) 258-5708.

All the authors declare no conflict of interest.

al., 2011; Shima*, et al.*, 2012). Bacterial CDTs are generally recognized as an AB_2-type toxin consisting of three subunits A, B, and C except for *S. enterica* serovarTyphi which has only CdtB (Haghjoo & Galan, 2004; Guerra*, et al.*, 2011). CdtB, after delivery into the target cells with the aid of CdtA and CdtC, utilizes its DNase I-like activity to induce limited host DNA damage (such as DSBs and SSBs) and thereby activate DNA repair responses (Guerra*, et al.*, 2011). Recently, it has been documented that *A. actinomycetemcomitans* CdtB can function as a phosphatidylinositol-3,4,5-triphosphate (PIP3) phosphatase which potentially perturbs the phosphoinositide 3-kinase signaling pathway that plays an important role in cell survival and growth (Scuron*, et al.*, 2016; Shenker*, et al.*, 2016). Several reports shows that CDTs are required for bacterial colonization, aggravate gastroenteritis, enhance inflammatory bowel disease, and promote progression of hepatic inflammation to preneoplastic dysplasia in mouse models of infection with CDT-producing *C. jejuni*, *H. hepaticus* and *H. cinaedi* (Fox*, et al.*, 2004; Young*, et al.*, 2004; Ge*, et al.*, 2005; Pratt*, et al.*, 2006; Ge*, et al.*, 2007; Shen*, et al.*, 2009). However, the direct link of CDT-induced DNA damage to intestinal carcinogenesis using in vivo models requires further study.

CDT-producing *H. hepaticus,* a close relative of human bacterial pathogens *Helicobacter pylori* and *C. jejuni,* is the prototype of enterohepatic helicobacters (Suerbaum*, et al.*, 2003; Fox*, et al.*, 2011). *H. hepaticus* infection induces chronic active hepatitis, hepatocellular tumors, typhlocolitis and lower bowel cancer in susceptible strains of immune-competent and immune-compromised mice (Fox*, et al.*, 1994; Fox*, et al.*, 1996; Erdman*, et al.*, 2003; Ge*, et al.*, 2007; Erdman*, et al.*, 2009; Fox*, et al.*, 2011). We previously reported that HhCDT is essential for maintaining persistent colonization in the intestine and promoting progression of inflammation to dysplasia in the liver (Ge*, et al.*, 2005; Ge*, et al.*, 2007). In this study, the role of the HhCDT in promoting the intestinal carcinogenesis of *H. hepaticus* infection was investigated in 129/SvEv *Rag2*$^{-/-}$ (129 *Rag2*$^{-/-}$15) mice.

Results

The presence of HhCDT promoted progression of intestinal preneoplastic lesions but did not influence the severity of *H. hepaticus*-induced inflammation over the course of infection

The cecum along with the ileo-ceco-colic (cecum/ICC) junction was assessed for various histopathological criteria, including inflammation, edema, epithelial defects, atrophy, hyperplasia and dysplasia with scores of ascending 1 to 4, and the cumulative score was presented as histopathologic activity index (HAI) (Erdman*, et al.*, 2009). At 10 WPI, the scores of inflammation, epithelial defects, crypt atrophy and dysplasia were significantly higher in the infected mice compared to the controls (Figure 1A, $P<0.05$ or less). There was no significant difference in the scores of all these categories between Hh-infected and the HhCDT mutant-infected mice (Figure 1, $P>0.5$). At 20 WPI, the Hh-infected mice had higher scores of all the categories except for epithelial defects and the HhCDT mutant-infected mice had higher scores of inflammation and dysplasia when compared with the controls (Figure 1B, $P<0.05$ or less). The Hh-infected mice developed more severe lesions of edema, atrophy, hyperplasia and dysplasia (all $P<0.05$) and epithelial defects with trend ($P=0.06$) except of inflammation ($P=0.34$) compared with the HhCDT mutant-infected mice

(Figure 1B). Similarly, the HAI scores representing the degrees of the overall pathological changes were significantly higher in Hh-infected mice compared with sham controls at both 10 and 20 WPI, whereas the HhCDT mutant-infected mice had significantly higher HAI scores at 10 WPI but not at 20 WPI compared with the controls (Figure 2A). Hh-infected mice had the average HAI score comparable to that in the HhCDT mutant-infected mice at 10 WPI (P=0.54), but significantly higher at 20 WPI (Figure 2A, P<0.02). Over the course of infection from 10 WPI to 20 WPI, infection with Hh (P=0.02) but not with the CDT mutant (P=0.21) promoted the progression of dysplastic lesions from 10 WPI to 20 WPI (Figure 2B); in contrast, the scores of inflammation were comparable between the infected groups or between time-points (Figure 2B, P>0.18). At 20 WPI, the Hh-infected mice developed multifocal to coalescing inflammation with prominent epithelial defects, mild edema, moderate to severe diffuse hyperplasia and high grade intra-epithelial neoplasia (GIN) with infrequent invasion of dysplastic cystic glands into the muscularis mucosa (2/4) and/or submucosa (2/4), thus classifying as invasive carcinoma (Figure 2C). In contrast, the cecum/ICC junction of the HhCDT mutant-infected mice developed moderate to severe inflammation, hyperplasia, epithelial defects with multifocal moderate dysplasia (3/5) or intraepithelial neoplasia (GIN) (2/5) but no invasive carcinoma. (Figure 2C). Thus, all of 4 Hh-infected mice developed intestinal carcinoma, whereas none of 5 HhCDT mutant-infected mice had carcinoma 20 WPI. Taken together, these data indicate that the HhCDT did not affect the severity of Hh-induced inflammation, but was essential for promoting the progression of preneoplastic dysplasia to cancer in this mouse model.

Pathological changes in the proximal/transverse colon and distal colon were also assessed using the same criteria for the cecum/ICC junction. The HAI scores in both of the colonic segments were significantly lower than those in the ceca in Hh-infected mice at both time points and in the HhCDT mutant-infected mice at 10 WPI (P<0.05). The infected mice had significantly higher colonic HAI scores compared with the controls at both time-points (Figure S1). However, there was no significant difference in the HAI scores or the scores of inflammation and dysplasia in the colon between Hh-infected and the HhCDT mutant-infected mice at both 10 and 20 WPI. Thus, the following research focused on the cecum/ICC junction.

Lack of HhCDT did not affect the colonization efficiency of the HhCDT mutant at both time points

We and others previously reported that the HhCDT mutants lose their colonization efficiency over time in outbred Swiss Webster mice, inbred A/JCr mice and C57BL/6 *Il-10*$^{-/-}$ mice (Ge*, et al.*, 2005; Pratt*, et al.*, 2006; Ge*, et al.*, 2007). We asked whether CDT played a role in *H. hepaticus* colonization in the cecum of 129*Rag2*$^{-/-}$ mice using qPCR (Figure 3). Both the HhCDT mutant and Hh persistently and efficiently colonized the cecum; there was no significant difference in colonization levels between Hh and the HhCDT mutant at 10 WPI (P=0.41) and 20 WPI (P=0.23) or between time points (P>0.1). These results indicated that the differences of pathological severity in the cecum/ICC junction between Hh and the HhCDT mutant did not result from the altered colonization efficiency of the HhCDT mutant.

The presence of CDT increased the ability of *H. hepaticus* to induce DSBs in epithelial cells

DNA damage induced by pathogens, mutagenic insults or reactive oxygen molecules plays a critical role in initiating tumor development (Hanahan & Weinberg, 2011). DNA double-strand breaks (DSBs) are one of the most toxic forms of DNA damage; unrepaired or incorrectly repaired DSBs can lead to genomic instability (Hanahan & Weinberg, 2011; Lord & Ashworth, 2012). Generation of DSBs results in the rapid phosphorylation of histone H2A variant H2AX at Ser139, termed γ-H2AX, which correlates with each DSB. The presence of γ-H2AX is the most sensitive marker for detecting DNA damage and the subsequent repair of the DNA lesions (Kuo & Yang, 2008). It has established that bacterial CDTs have DNase I-like activity that can induce host chromosomal fragmentation and elicit DNA damage repair responses (Guerra*, et al.*, 2011). Treatment of recombinant HhCDT increased the production of γ-H2XA in INT407 cells, indicating the ability of HhCDT in inducing DSBs (Liyanage*, et al.*, 2010). We employed γH2XA staining to assess whether the lack of CDT affects the ability of *H. hepaticus* to cause host DNA damage. In the infected mice, the majority of γ-H2XA foci^{+} cells originated from glands in proximity to the glands undergoing dysplastic areas surrounded by infiltration of inflammatory cells. Macrophages and neutrophils were the major types of inflammatory cells noted by co-staining using anti-γ-H2XA antibody with either anti-F4/80 for macrophage or anti-MPO for neutrophils (Figure S2A and B). There were very few γ-H2XA-positive cells in the cecum/ICC junction of uninfected controls compared with the infected mice at both time-points (Figure 4B, P<0.001). HhCDT-deficiency significantly decreased the numbers of γ-H2XA foci^{+} cells in the cecum/ICC junction compared with Hh-infected mice at 10 (P<0.028) and 20 (P<0.013) WPI. These results indicated that HhCDT played an important role in enhancing *in vivo* genotoxic effects induced by Hh infection.

HhCDT enhanced transcription of cecal proinflammatory *Il-6* and *Tnfa* but reduced expression of anti-inflammatory cytokine *Il-10* at 10 WPI

To shed light on the signaling pathways possibly involved in HhCDT-induced progression of intestinal carcinogenesis, we measured mRNA levels of selected genes that have been implicated in promoting carcinogenesis. At 10 WPI, infection with Hh significantly increased the mRNA levels of *Tnf*-α ($P = 0.026$), *Il-6* (P=0.028), but decreased mRNA levels of *Il-10* (P=0.038) when compared to the HhCDT mutant in the cecum (Figure 5A). In contrast, there was no significant difference in the mRNA levels of *Ifn*-γ, *IL-1*β*, Il-22,* and *Cxcl1* ($P > 0.4$) between the Hh- and HhCDT mutant-infected mice at 10 WPI (Figure 5B). Also at 20 WPI, there was no significant difference in mRNA levels of these cytokines between the Hh- and HhCDT mutant-infected mice (Figure 5A and B). When compared to the sham controls, the ceca of mice infected with Hh or HhCDT mutant contained higher mRNA levels of these tested cytokines including *Tnf*-α, *Il-10*, *Ifn*-γ, *IL-1*β*, Il-22,* and *Cxcl1* (all $P < 0.05$ or less) at 10 WPI, whereas mRNA expression of all the target cytokines except for *Il-10* and *Il-6* were significantly up-regulated at 20 WPI (Figure 5A and B, P<0.05 or less). These data suggested that HhCDT enhanced transcriptional up-regulation of a subset of proinflammatory cytokines *Il-6* and *Tnf*-α, and suppressed expression of an anti-inflammatory cytokine *Il-10* during the early stage of infection.

Activation of Stat3 was elevated by infection with Hh compared with the HhCDT mutant

Cumulative evidence indicate that activation of Stat3 regulates multiple cellular signaling pathways involved in tumor proliferation, survival, angiogenesis, invasion, inflammation and metastasis (Yu, *et al.*, 2009; Siveen, *et al.*, 2014). Stat3 can be activated via phosphorylation by diverse stimuli including Il-6 and Tnfα (Siveen, *et al.*, 2014). Since transcription of cecal *Il-6* and *Tnfα* was increased by Hh when compared to the HhCDT mutant, the phospho-Stat3^{+} epithelial cells in the cecum/ICC junction were examined by using immunohistochemistry and compared between Hh- and HhCDT mutant-infected mice (Figure 6). We noted that the phospho-Stat3 positivity was gland-based; all the epithelial cells in the same gland were either phospho-Stat3-positive or –negative; in the infected mice, the phospho-Stat3 foci^{+} epithelial cells occurred adjacent to the inflamed areas (Figure 6B), which were infiltrated by macrophages and neutrophils (Figure S2A and B) . There was fewer phospho-Stat3 foci^{+} epithelial glands in the controls; the index of the Stat3 activation was significantly greater in the infected mice compared to the controls at both time points (Figure 6B, $P<0.0001$). The phospho-Stat3 foci^{+} index were comparable between HhCDT mutant- and Hh-infected groups at 10 WPI (Figure 6B, $P=0.54$), but the Stat3 activation was significantly enhanced in Hh-infected mice compared with the HhCDT mutant-infected mice at 20 WPI (Figure 6B, $P< 0.02$). These results were consistent with the finding that Hh infection induced more severe dysplasia compared to mice infected with the HhCDT mutant (Figure 2B, $P<0.03$). Linear regression analysis revealed that there was a strong positive correlation between intensity of the phospho-Stat3^{+} signal and scores of dysplasia (Figure 4C, $P<0.0001$, $R^2=0.83$). Taken together, these data suggested that HhCDT elevated Stat3 activation and played an important role in Hh-induced intestinal carcinogenesis.

Discussion

It has been established that bacterial CDTs, classified as an AB_2 toxin, provoke cytopathic effects on cultured mammalian cells via a cascade of cellular responses including induction of DNA damage, activation of DNA damage repair mechanisms, cell growth arrest, and dysregulation of pro-oncogenic signaling pathways (Guerra, *et al.*, 2011). However, *in vivo* pathogenic potential of CDTs in bacterial infection are not fully appreciated, despite some progress in elucidating its pathogenic potential (Ge, *et al.*, 2008; Guerra, *et al.*, 2011). In this study, we demonstrated that HhCDT promoted progression of preneoplastic lesions to carcinoma over 20 weeks of *H. hepaticus* infection and upregulated transcription of cecal *Il-6* and *Tnfα* in the early stage of infection. Additionally, the lack of HhCDT decreased the ability of *H. hepaticus* to induce DNA damage and to activate Stat3 signaling, but did not affect colonization efficiency in 129*Rag2*$^{-/-}$ mice. Taken together, these data suggested that HhCDT enhances carcinogenic potential of *H. hepaticus* at least in part via elevation of DSBs and increased activation of the Tnfα/Il-6-Stat3 signaling.

Beside CDTs, few other bacterial toxins are reported to directly involve induction of DNA damage on the host nuclear DNA. Select commensal and pathogenic *E. coli* strains harbor a genomic island *pks* which encodes genotoxic colibactin (Nougayrede, *et al.*, 2006). Like CDT, colibactin can induce DSBs and G2/M cell arrest in cultured mammalian cells (Nougayrede, *et al.*, 2006).When compared to wild type *pks+ E. coli* NC101, colibactin-

deficient *E. coli* NC101 decreased the number of γH2AX foci^{+} cells and attenuated tumorigenicity, but did not affect intestinal inflammation in AOM-treated C57BL/6*Il-10*$^{-/-}$ mice (Arthur, *et al.*, 2012). Consistent with these findings, the HhCDT mutant in this study maintained its ability to elicit intestinal inflammation, induce expression of proinflammatory cytokines, including *Il-1β, Infγ* and *Il-22*, but lost the potential to promote the progression of preneoplastic dysplasia to carcinoma from 10 WPI to 20 WPI compared with Hh-infected 129*Rag2*$^{-/-}$ mice. In addition, in our previous study, infection with the same HhCDT mutant induced less severe hepatic dysplasia, but retained similar degrees of hepatitis compared with Hh infection in male A/JCr mice (Ge, *et al.*, 2007). It was also reported that C57BL/6 *Il10*$^{-/-}$ mice infected with an independent HhCDT-deficient isogenic *H. hepaticus* mutant 3B1::Tn*20* developed less severe typhlocolits compared with CDT-positive *H. hepaticus*-infected mice (Young, *et al.*, 2004; Pratt, *et al.*, 2006). Moreover, CDT inactivation in *C. jejuni* and *H. cinaedi,* both of which are genetically close relatives of *H. hepaticus*, ameliorate gastric dysplasia in NF-κB-deficient 3X mice (129 X C57BL/6 *p50*$^{-/-}$*p65*$^{+/}$12) and colitis in C57BL/6*Il-10*$^{-/-}$ mice, respectively (Fox, *et al.*, 2004; Shen, *et al.*, 2009). It is worth noting that severity of inflammation in the stomach of the *C. jejuni* CDT mutant-infected 3X mice and in the intestine of *H. cinaedi* CDT mutant-infected C57BL/129*Il-10*$^{-/-}$ mice were also attenuated. The differential roles of CDTs in inflammation between these studies and our study likely resulted from two major factors: (1) the use of different mouse models that vary in genetic backgrounds, host immunity, and different gastrointestinal microbiota; (2) certain virulence properties of CDTs among bacterial species may be different. Nevertheless, these data collectively indicate that bacterial genotoxin-induced DNA damage could serve as a tumor promotor in both the hepatic and gastrointestinal tracts.

Activation of Stat3 signaling can lead to expression of a large array of oncogenic and inflammatory factors that are crucial for cell survival and proliferation, invasion, metastasis and angiogenesis.(Siveen, *et al.*, 2014; Yu, *et al.*, 2014). Stat3 can be activated by diverse agents including growth factors and cytokines such as Il-6 and Tnfα (Siveen, *et al.*, 2014; Yu, *et al.*, 2014). In the current study, the presence of HhCDT increased expression of cecal *Il-6* and *Tnf-α* at 10 WPI, and elevated activation of Stat3 at 20 WPI. The elevated activation of Stat3 is in concert with more severe preneoplastic lesions in Hh-infected mice compared with the HhCDT mutant-infected mice. Enhancement of the Tnf-α/Il-6-Stat3 has been associated with bacterial biofilm-covered human colon tumors (Dejea, *et al.*, 2014). In a syngeneic B16 melanoma cell tumor model of C57BL/6*Ifn-γ*$^{-/-}$ mice, blockage of Il-6 production resulted in suppression of the Stat3 activation and significantly inhibited tumor growth (Wang, *et al.*, 2009). DNA damage in HCT116 human colon cancer cells induced by doxorubicin (causing DNA breaks via inhibition of DNA strand resealing) increased the Il-6 production, and phosphorylation of Stat3, which was abolished with treatment of anti-Il-6 antibody (Yun, *et al.*, 2012). A recent study indicated that Il-6 and Tnfα synergistically activate Stat3 and NF-kB to promote colorectal cancer cell growth (De Simone, *et al.*, 2015). These lines of evidence suggest that the Tnfα/Il-6-stat3 signaling plays an important role in HhCDT-induced promotion of intestinal tumorigenesis.

The critical role of the Stat3 signaling in inflammation-driven colonic carcinogenesis has been demonstrated in mouse models of colitis-associated cancer {Bollrath, 2009 #221;rivennikov, 2009 #223}. Treatment with AOM and DSS caused lower tumor

multiplicity and smaller tumor sizes in Stat3-deficient C57BL/6 mice compared to wild-type counterparts; elevation of Stat3 signaling was induced by Il-6 and gp130 (Bollrath, *et al.*, 2009; Grivennikov, *et al.*, 2009). Additionally, the classical NF-κB pathway also played a pivotal role in promoting inflammation-driven colonic carcinogenesis in the same model (Greten, *et al.*, 2004). These findings have linked inflammation and intestinal tumorigenesis (Taniguchi & Karin, 2014). Similarly, we previously reported that anti-inflammatory treatments with Il-10-Ig fusion protein or anti-Tnfα antibody ameliorated severity of intestinal inflammation and carcinoma in Hh-infected 129*Rag2*$^{-/-}$ mice, indicating that inflammation is also integral in promoting Hh-induced intestinal tumorigenesis(Erdman, *et al.*, 2003; Erdman, *et al.*, 2009). Our recent study demonstrated that depletion of a potent inflammatory mediator Il-22 in Hh-infected 129*Rag2*$^{-/-}$ mice significantly inhibited inflammation, hyperplasia and dysplasia in the cecum and the colon and also decreased the number of γH2AX foci^{+} cells compared to untreated Hh-infected counterparts at 10 WPI (Wang, *et al.*, 2017). Thus, our data collectively indicate that both inflammation and HhCDT are required for potentiating carcinogenic potency of Hh. We propose a working model in which a cascade of cellular events occurs during HhCDT-induced progression of intestinal carcinogenesis: HhCDT in *H. hepaticus* increases the host DNA damage by inducing DSBs that can upregulate the expression of *Il-6* and *Tnfα*. This upregulation subsequently enhances activation of Stat3 which promotes intestinal carcinogenesis. Intriguingly, we found that HhCDT-deficiency was associated with increased transcription of cecal *Il-10*. Il-10 is an anti-inflammatory, pleiotropic cytokine that plays paradoxical roles in tumor inhibition and tumor promotion, and also can induce activation of Stat3 (Yu, *et al.*, 2014; Mannino, *et al.*, 2015). It has been documented that Il-10 is indispensable for regulatory T cells-mediated suppression of Hh-induced carcinogenesis in 129*Rag2*$^{-/-}$ mice (Erdman, *et al.*, 2003; Erdman, *et al.*, 2009). Additionally, Il-10-deficiency in 129*Rag2*$^{-/-}$ mice increased Hh-induced carcinoma incidence, whereas treatment with exogenous Il-10 suppressed the development of intestinal carcinoma (Erdman, *et al.*, 2009; Fox, *et al.*, 2011). The finding that the association of the attenuated ileocecocolic dysplasia with upregulation of cecal *Il-10* in the HhCDT mutant-infected mice suggests that Il-10 plays a role in ameliorating Hh-induced intestinal disease, but not in activating the Stat3 signaling pathway.

Our previous studies indicated that HhCDT is essential for long-term persistent Hh intestinal colonization in the intestine of immunocompetent Swiss Webster and A/JCr mice (Ge, *et al.*, 2005; Ge, *et al.*, 2007). In contrast, the same HhCDT mutant used in this study had intestinal colonization levels comparable to Hh in 129*Rag2*$^{-/-}$ mice. This discrepancy is likely due to the use of different mouse models that confer differential immunity against *H. hepaticus* infection; Swiss Webster and A/JCr mice are immune-component, whereas 129*Rag2*$^{-/-}$ mice lacking mature T and B cells are deficient in adaptive immunity. In addition, another study indicated that the *H. hepaticus* CDT mutant 3B1::Tn*20* was progressively eliminated from the lower bowel over 32 WPI (Pratt, *et al.*, 2006). Moreover, CjCDT is essential for persistent colonization of *C. jejuni* in C57BL/6 mice, but is not required in NF-κB-deficient 3X mice (Fox, *et al.*, 2004). It is also worth noting that *H. cinaedi* CDT plays an important role in promoting typhlocolitis but is dispensable for bacterial colonization in C57BL/6 *Il10*$^{-/-}$ mice for a period of 12 weeks (Shen, *et al.*, 2009). The mechanisms underlying the

differential roles of CDTs in colonization among CDT-producing bacteria require further studies.

Interestingly, HhCDT promoted the progression of tumorigenesis only in the cecum/ileocecocolic junction, but not in the colon. It has been documented that Hh infection induced the most severe pathology in the ileocecocolic junctions in *Rag2*-deficient mice (129/SvEv or C57BL/6 backgrounds) and C57BL/6 *Il10*$^{-/-}$ mice (Erdman, *et al.*, 2003; Kullberg, *et al.*, 2006; Mangerich, *et al.*, 2012). Consistent with these previous findings, in the Hh-infected mice there was more severe pathology in the ceca and ileocecocolic junction compared with transverse and distal colon at both time-points and in the HhCDT mutant-infected mice at 10 WPI. In addition, previous studies in anti-Il10R-teated C57BL/6 mice reported that Il-22 and Ifnγ are required for inducing colonic inflammation but not for cecal inflammation by *H. hepaticus*, whereas anti-Il-17 treatment increased severity of cecal pathology but not colonic pathology (Kullberg, *et al.*, 2006; Morrison, *et al.*, 2015). Thus, it is possible that the progression of preneoplastic dysplasia to cancer promoted by HhCDT requires a host factor(s) and a defined microflora only present in the ceca and ileocecocoloic junction.

DNA damage such as DSB and SSB, when unrepaired or incorrectly repaired, can lead to mutation and genomic instability, one of the most pervasive characteristics of cancer cells (Hanahan & Weinberg, 2011). We demonstrated the role of HhCDT in promoting intestinal carcinogenesis by linking its DNA damage ability to progression of preneoplastic dysplasia to cancer. HhCDT-dependent upregulation of *Il-6* and *Tnf-α* transcription associated with increased activation of Stat3 highlights the potential importance of the Tnf-α/Il-6-Stat3 signaling pathway in HhCDT-mediated tumor promotion. In addition, enhanced expression of Il-6/Tnf-α is also correlated with the activation of the classical NF-κB pathway in HhCDT-dependent promotion of hepatocarcinogenesis (Ge, *et al.*, 2007; Pere-Vedrenne, *et al.*, 2016). Since there are closely linked interactions between Stat3 signaling and the NF-κB pathway in cancer cells, various cancer therapies targeting these signaling pathways are actively being developed (Siveen, *et al.*, 2014). Given the role of HhCDT in promoting liver and intestinal tumorigenesis, the contribution of bacterial CDTs to pathogenicity of human enteric bacterial pathogens expressing CDT such as *Campylobacter* sp., *S. enterica* serovar Typhi, *Shigella dysenteriae* and *Escherichia coli* strains warrants future investigations.

Materials and Methods

Bacterial strains and Experimental Infection

Twenty-four, 4 to 6-week-old 129/SvEv *Rag2*$^{-/-}$ mice of both sexes (13 males and 11 females) were produced from the in-house colony maintained under specific-pathogen-free (SPF) conditions (free of *Helicobacter* spp., *Citrobacter rodentium*, *Salmonella* spp., endoparasites, ectoparasites, and exogenous murine viral pathogens) in an Association for Assessment and Accreditation of Laboratory Animal Care International (AAALAC International)-accredited facility at Massachusetts Institute of Technology as described previously (Erdman, *et al.*, 2003; Erdman, *et al.*, 2009)}. Mice were housed at 70 ± 2°F, in 30 to 70% relative humidity, and in a 12-h/12-h light/dark cycle and were fed standard

rodent chow (Purina Mills, St. Louis, MO) and water *ad libitum*. Animal use was approved by the MIT Committee on Animal Care.

Three groups of 7 to 9 mice (mixed sexes) were dosed with *H. hepaticus* strain 3B1 (Hh, n=8) (ATCC51448), the *cdtB*-deficient *H. hepaticus* mutant HhcdtBm7 (HhCDT mutant, n=9) lacking CDT activity or sham-dosed with Brucella broth as a control (n=7), respectively. Generation of HhcdtBm7 and culture conditions for Hh and the mutant were previously described (Ge*, et al.*, 2005). Mice received 0.2 ml of fresh inocula containing ~2 × 10^8 organisms or vehicle alone as control by gastric gavage every other day for three inoculations. Mice, 3 and 4 for controls, 4 and 4 for Hh infection, 4 and 5 for the HhCDT infection, were necropsied at 10 and 20 weeks post Hh inoculation (WPI), respectively.

Necropsy and histopathology

For necropsy, the cecum including the ileocecocolic junction (ICC/Cecum), proximal/transverse colon and distal colon were collected for routine histological processing and sectioning, respectively. The collected tissues were embedded in paraffin, sectioned at 4 μm and stained with hematoxylin and eosin, and were examined independently by two boarded veterinary pathologists (NP and SM) blinded to sample identity for inflammation, edema, epithelial defects, crypt atrophy, hyperplasia, and dysplasia as previously described (Boivin*, et al.*, 2003; Erdman*, et al.*, 2003). An intestinal histologic activity index (HAI) for cecum and colon was generated by combining scores for all categorical lesion scores for a particular intestinal segment.

qPCR for quantitating *H. hepaticus* colonization and gene expression

For quantifying *H. hepaticus* levels, chromosomal DNA from the cecal tissues was prepared using a High Pure PCR Template kit according to the manufacturer's protocol (Roche Applied Science, Indianapolis, IN). Levels of ceal *H. hepaticus* were measured by qPCR in the 7500 Fast Real-Time PCR System (Life Technologies, Carlsbad, CA) as described elsewhere (Ge*, et al.*, 2001; Ge*, et al.*, 2005). The genomic numbers of *H. hepaticus* were then normalized to μg of mouse chromosomal DNA whose quantities in the samples were determined by qPCR using the 18S rRNA gene-based primers and probe mixture (Life Technologies) as described previously (Ge*, et al.*, 2005).

For measuring mRNA levels of target genes, total RNA from ceca were isolated using Trizol Reagents following the supplier's procedure (Invitrogen, Carlsbad, CA). Five μg of the total RNA from samples were converted into cDNA using the High Capacity cDNA Archive kit (Life Technology). Levels of *Ifn*-γ, *IL-6*, *Il-1*β, *Tnf*-α, *Il-10, Il-22,* and *Cxcl1* mRNA were measured by qPCR using commercial primers and probes in the 7500 Fast Real-Time PCR System (Life Technologies). Transcript levels were normalized to the endogenous control glyceraldehyde-3-phosphate dehydrogenase mRNA (*Gapdh*), and expressed as fold change compared with sham-dosed control mice using the Comparative C_T method (Applied Biosystems User Bulletin no. 2).

Immunohistochemistry

Formalin-fixed cecum sections (4 μm thick) were processed and stained with γH2AX monoclonal antibody (mAb), a biomarker for double DNA strand breaks (DSBs), phospho (Tyr705)-Stat3 mAb as previously described (Shen*, et al.*, 2016). Briefly, the tissue sections were deparaffinized and rehydrated in graded ethanol concentrations and then were immersed in low-pH (γH2AX staining) or high-pH (phospho-Stat3 staining) target retrieval solution (Dako, Carpinteria, CA, USA) in a 95°C water bath for 20 min. The slides were incubated with mAb either for γH2AX (1:200 dilution, Cat#9718) or for phospho-Stat3 (1:100 dilution, Cat#9145) (Cell Signaling, Danvers, MA, USA), followed by incubation with Alexa Fluor 488- or 594-conjugated anti-rabbit $F(ab')_2$ fragment (Cell Signaling). The cell nuclei were stained using 10 μl of Prolong Gold antifade reagent with DAPI (Cell Signaling). The tissue sections were visualized using a Zeiss Axioskop 2 Plus microscope (Zeiss, Germany). Cells possessing one or more γ-H2AX foci$^+$ were counted as positive; index of the γH2AX foci$^+$ epithelial cells were expressed as the average percentage of the γH2AX-postive cells to the total epithelial cells based on 8 images per mouse at 40X magnification. The index of the phosph-Stat3-positive epithelial cells were expressed as percentage of phospho-Stat3 foci$^+$ crypts to total glands (50–100 glands per mouse). To examine phenotypes of inflammatory cells associated with γH2AX foci$^+$ epithelial cells, representative ceca of each group were also co-stained with anti-γH2AX antibody for DBSs (anti-rabbit, Cat#9718) and anti F4/80 antibody for macrophages (anti-rat, Abcam, Cat# ab6640) or anti-γH2AX antibody for DSBs (anti-mouse, Millipore, Cat# JBW301) and anti-myeloperoxidase (MPO) antibody for neutrophils (anti-rabbit, Abcam, Cat# ab45977). The stained slides were incubated with the corresponding Alex-Fluor-488 conjugated secondary antibody (green) and Alex-Fluor-568 conjugated antibody (red) according to the origin of the first antibodies.

Statistical analysis

All statistical analyses were conducted using the Prism software Package 6.01 (Graphpad, San Diego, CA). Intestinal HAI scores and categorical lesions were compared across groups by the one-way ANOVA test with Bonferroni's Multiple Comparison Test, and between groups by the two-tailed Mann-Whitney *U*-test. Data on the colonization levels of *H. hepaticus,* cytokine mRNA levels, the index for γH2XA foci$^+$ and phosph-Stat3 foci$^+$ staining in the tissues were analyzed using the two-tailed Student's *t* test. Correlation between scores of dysplasia and the phospho-Stat3 foci$^+$ index was performed using linear regression analysis. Values of $P<0.05$ were considered significant.

Supplementary Material

Refer to Web version on PubMed Central for supplementary material.

Acknowledgments

This study was supported in part by NIH grants R01-OD01141, T32-OD010978, and P01 CA28842 (to JGF).

We thank Christian Kaufman and Lenzy Cheaney for mice manipulation and care, Guanyu Gong for assistance with immunohistochemistry, and Alyssa Terestre Pappa for preparation of manuscript.

References

Arthur JC, Perez-Chanona E, Muhlbauer M, Tomkovich S, Uronis JM, Fan TJ, … Jobin C. Intestinal inflammation targets cancer-inducing activity of the microbiota. Science. 2012; 338:120–123. [PubMed: 22903521]

Boivin GP, Washington K, Yang K, Ward JM, Pretlow TP, Russell R, … Coffey RJ. Pathology of mouse models of intestinal cancer: consensus report and recommendations. Gastroenterology. 2003; 124:762–777. [PubMed: 12612914]

Bollrath J, Phesse TJ, von Burstin VA, Putoczki T, Bennecke M, Bateman T, … Greten FR. gp130-mediated Stat3 activation in enterocytes regulates cell survival and cell-cycle progression during colitis-associated tumorigenesis. Cancer Cell. 2009; 15:91–102. [PubMed: 19185844]

De Simone V, Franze E, Ronchetti G, Colantoni A, Fantini MC, Di Fusco D, … Stolfi C. Th17-type cytokines, IL-6 and TNF-alpha synergistically activate STAT3 and NF-kB to promote colorectal cancer cell growth. Oncogene. 2015; 34:3493–3503. [PubMed: 25174402]

Dejea CM, Wick EC, Hechenbleikner EM, White JR, Mark Welch JL, Rossetti BJ, … Sears CL. Microbiota organization is a distinct feature of proximal colorectal cancers. Proc Natl Acad Sci U S A. 2014; 111:18321–18326. [PubMed: 25489084]

Erdman SE, Rao VP, Poutahidis T, Ihrig MM, Ge Z, Feng Y, … Fox JG. CD4(+)CD25(+) regulatory lymphocytes require interleukin 10 to interrupt colon carcinogenesis in mice. Cancer Res. 2003; 63:6042–6050. [PubMed: 14522933]

Erdman SE, Rao VP, Poutahidis T, Rogers AB, Taylor CL, Jackson EA, … Fox JG. Nitric oxide and TNF-alpha trigger colonic inflammation and carcinogenesis in Helicobacter hepaticus-infected, Rag2-deficient mice. Proc Natl Acad Sci U S A. 2009; 106:1027–1032. [PubMed: 19164562]

Fox JG, Ge Z, Whary MT, Erdman SE, Horwitz BH. Helicobacter hepaticus infection in mice: models for understanding lower bowel inflammation and cancer. Mucosal Immunol. 2011; 4:22–30. [PubMed: 20944559]

Fox JG, Li X, Yan L, Cahill RJ, Hurley R, Lewis R, Murphy JC. Chronic proliferative hepatitis in A/JCr mice associated with persistent Helicobacter hepaticus infection: a model of *helicobacter*-induced carcinogenesis. Infect Immun. 1996; 64:1548–1558. [PubMed: 8613359]

Fox JG, Rogers AB, Whary MT, Ge Z, Taylor NS, Xu S, … Erdman SE. Gastroenteritis in NF-kappaB-deficient mice is produced with wild-type *Camplyobacter jejuni* but not with *C. jejuni* lacking cytolethal distending toxin despite persistent colonization with both strains. Infect Immun. 2004; 72:1116–1125. [PubMed: 14742559]

Fox JG, Dewhirst FE, Tully JG, Paster BJ, Yan L, Taylor NS, … Ward JM. *Helicobacter hepaticus* sp. nov., a microaerophilic bacterium isolated from livers and intestinal mucosal scrapings from mice. J Clin Microbiol. 1994; 32:1238–1245. [PubMed: 8051250]

Ge Z, Schauer DB, Fox JG. In vivo virulence properties of bacterial cytolethal-distending toxin. Cell Microbiol. 2008; 10:1599–1607. [PubMed: 18489725]

Ge Z, White DA, Whary MT, Fox JG. Fluorogenic PCR-based quantitative detection of a murine pathogen, Helicobacter hepaticus. J Clin Microbiol. 2001; 39:2598–2602. [PubMed: 11427576]

Ge Z, Rogers AB, Feng Y, Lee A, Xu S, Taylor NS, Fox JG. Bacterial cytolethal distending toxin promotes the development of dysplasia in a model of microbially induced hepatocarcinogenesis. Cell Microbiol. 2007; 9:2070–2080. [PubMed: 17441986]

Ge Z, Feng Y, Whary MT, Nambiar PR, Xu S, Ng V, … Fox JG. Cytolethal distending toxin is essential for *Helicobacter hepaticus* colonization in outbred Swiss Webster mice. Infect Immun. 2005; 73:3559–3567. [PubMed: 15908385]

Greten FR, Eckmann L, Greten TF, Park JM, Li ZW, Egan LJ, … Karin M. IKKbeta links inflammation and tumorigenesis in a mouse model of colitis-associated cancer. Cell. 2004; 118:285–296. [PubMed: 15294155]

Grivennikov S, Karin E, Terzic J, Mucida D, Yu GY, Vallabhapurapu S, … Karin M. IL-6 and Stat3 are required for survival of intestinal epithelial cells and development of colitis-associated cancer. Cancer Cell. 2009; 15:103–113. [PubMed: 19185845]

Guerra L, Cortes-Bratti X, Guidi R, Frisan T. The biology of the cytolethal distending toxins. Toxins (Basel). 2011; 3:172–190. [PubMed: 22069704]

Haghjoo E, Galan JE. *Salmonella typhi* encodes a functional cytolethal distending toxin that is delivered into host cells by a bacterial-internalization pathway. Proc Natl Acad Sci U S A. 2004; 101:4614–4619. [PubMed: 15070766]

Hanahan D, Weinberg RA. Hallmarks of cancer: the next generation. Cell. 2011; 144:646–674. [PubMed: 21376230]

Helleday T, Eshtad S, Nik-Zainal S. Mechanisms underlying mutational signatures in human cancers. Nat Rev Genet. 2014; 15:585–598. [PubMed: 24981601]

Kullberg MC, Jankovic D, Feng CG, Hue S, Gorelick PL, McKenzie BS, … Sher A. IL-23 plays a key role in Helicobacter hepaticus-induced T cell-dependent colitis. J Exp Med. 2006; 203:2485–2494. [PubMed: 17030948]

Kuo LJ, Yang LX. Gamma-H2AX - a novel biomarker for DNA double-strand breaks. In Vivo. 2008; 22:305–309. [PubMed: 18610740]

Liyanage NP, Manthey KC, Dassanayake RP, Kuszynski CA, Oakley GG, Duhamel GE. Helicobacter hepaticus cytolethal distending toxin causes cell death in intestinal epithelial cells via mitochondrial apoptotic pathway. Helicobacter. 2010; 15:98–107. [PubMed: 20402812]

Lord CJ, Ashworth A. The DNA damage response and cancer therapy. Nature. 2012; 481:287–294. [PubMed: 22258607]

Mangerich A, Knutson CG, Parry NM, Muthupalani S, Ye W, Prestwich E, … Dedon PC. Infection-induced colitis in mice causes dynamic and tissue-specific changes in stress response and DNA damage leading to colon cancer. Proc Natl Acad Sci U S A. 2012; 109:E1820–1829. [PubMed: 22689960]

Mannino MH, Zhu Z, Xiao H, Bai Q, Wakefield MR, Fang Y. The paradoxical role of IL-10 in immunity and cancer. Cancer Lett. 2015; 367:103–107. [PubMed: 26188281]

Morrison PJ, Ballantyne SJ, Macdonald SJ, Moore JW, Jenkins D, Wright JF, … Kullberg MC. Differential Requirements for IL-17A and IL-22 in Cecal versus Colonic Inflammation Induced by Helicobacter hepaticus. Am J Pathol. 2015; 185:3290–3303. [PubMed: 26458765]

Nougayrede JP, Homburg S, Taieb F, Boury M, Brzuszkiewicz E, Gottschalk G, … Oswald E. Escherichia coli induces DNA double-strand breaks in eukaryotic cells. Science. 2006; 313:848–851. [PubMed: 16902142]

Pere-Vedrenne C, Cardinaud B, Varon C, Mocan I, Buissonniere A, Izotte J, … Menard A. The Cytolethal Distending Toxin Subunit CdtB of Helicobacter Induces a Th17-related and Antimicrobial Signature in Intestinal and Hepatic Cells In Vitro. J Infect Dis. 2016; 213:1979–1989. [PubMed: 26908757]

Pratt JS, Sachen KL, Wood HD, Eaton KA, Young VB. Modulation of host immune responses by the cytolethal distending toxin of *Helicobacter hepaticus*. Infect Immun. 2006; 74:4496–4504. [PubMed: 16861635]

Scuron MD, Boesze-Battaglia K, Dlakic M, Shenker BJ. The Cytolethal Distending Toxin Contributes to Microbial Virulence and Disease Pathogenesis by Acting As a Tri-Perditious Toxin. Front Cell Infect Microbiol. 2016; 6:168. [PubMed: 27995094]

Shen Z, Feng Y, Rogers AB, Rickman B, Whary MT, Xu S, … Fox JG. Cytolethal distending toxin promotes Helicobacter cinaedi-associated typhlocolitis in interleukin-10-deficient mice. Infect Immun. 2009; 77:2508–2516. [PubMed: 19307212]

Shen Z, Mannion A, Whary MT, Muthupalani S, Sheh A, Feng Y, … Fox JG. Helicobacter saguini, a Novel Helicobacter Isolated from Cotton-Top Tamarins with Ulcerative Colitis, Has Proinflammatory Properties and Induces Typhlocolitis and Dysplasia in Gnotobiotic IL-10−/− Mice. Infect Immun. 2016; 84:2307–2316. [PubMed: 27245408]

Shenker BJ, Boesze-Battaglia K, Scuron MD, Walker LP, Zekavat A, Dlakic M. The toxicity of the Aggregatibacter actinomycetemcomitans cytolethal distending toxin correlates with its phosphatidylinositol-3,4,5-triphosphate phosphatase activity. Cell Microbiol. 2016; 18:223–243. [PubMed: 26247396]

Shima A, Hinenoya A, Asakura M, Sugimoto N, Tsukamoto T, Ito H, … Yamasaki S. Molecular characterizations of cytolethal distending toxin produced by Providencia alcalifaciens strains isolated from patients with diarrhea. Infect Immun. 2012; 80:1323–1332. [PubMed: 22252871]

Siveen KS, Sikka S, Surana R, Dai X, Zhang J, Kumar AP, … Bishayee A. Targeting the STAT3 signaling pathway in cancer: role of synthetic and natural inhibitors. Biochim Biophys Acta. 2014; 1845:136–154. [PubMed: 24388873]

Suerbaum S, Josenhans C, Sterzenbach T, Drescher B, Brandt P, Bell M, … Fox JG. The complete genome sequence of the carcinogenic bacterium *Helicobacter hepaticus*. Proc Natl Acad Sci U S A. 2003; 100:7901–7906. [PubMed: 12810954]

Taniguchi K, Karin M. IL-6 and related cytokines as the critical lynchpins between inflammation and cancer. Semin Immunol. 2014; 26:54–74. [PubMed: 24552665]

Wang C, Gong G, Sheh A, Muthupalani S, Bryant EM, Puglisi DA, … Horwitz BH. Interleukin-22 drives nitric oxide-dependent DNA damage and dysplasia in a murine model of colitis-associated cancer. Mucosal Immunol. 2017 Accepted.

Wang L, Yi T, Kortylewski M, Pardoll DM, Zeng D, Yu H. IL-17 can promote tumor growth through an IL-6-Stat3 signaling pathway. J Exp Med. 2009; 206:1457–1464. [PubMed: 19564351]

Young VB, Knox KA, Pratt JS, Cortez JS, Mansfield LS, Rogers AB, … Schauer DB. In vitro and in vivo characterization of *Helicobacter hepaticus* cytolethal distending toxin mutants. Infect Immun. 2004; 72:2521–2527. [PubMed: 15102759]

Yu H, Pardoll D, Jove R. STATs in cancer inflammation and immunity: a leading role for STAT3. Nat Rev Cancer. 2009; 9:798–809. [PubMed: 19851315]

Yu H, Lee H, Herrmann A, Buettner R, Jove R. Revisiting STAT3 signalling in cancer: new and unexpected biological functions. Nat Rev Cancer. 2014; 14:736–746. [PubMed: 25342631]

Yun UJ, Park SE, Jo YS, Kim J, Shin DY. DNA damage induces the IL-6/STAT3 signaling pathway, which has anti-senescence and growth-promoting functions in human tumors. Cancer Lett. 2012; 323:155–160. [PubMed: 22521547]

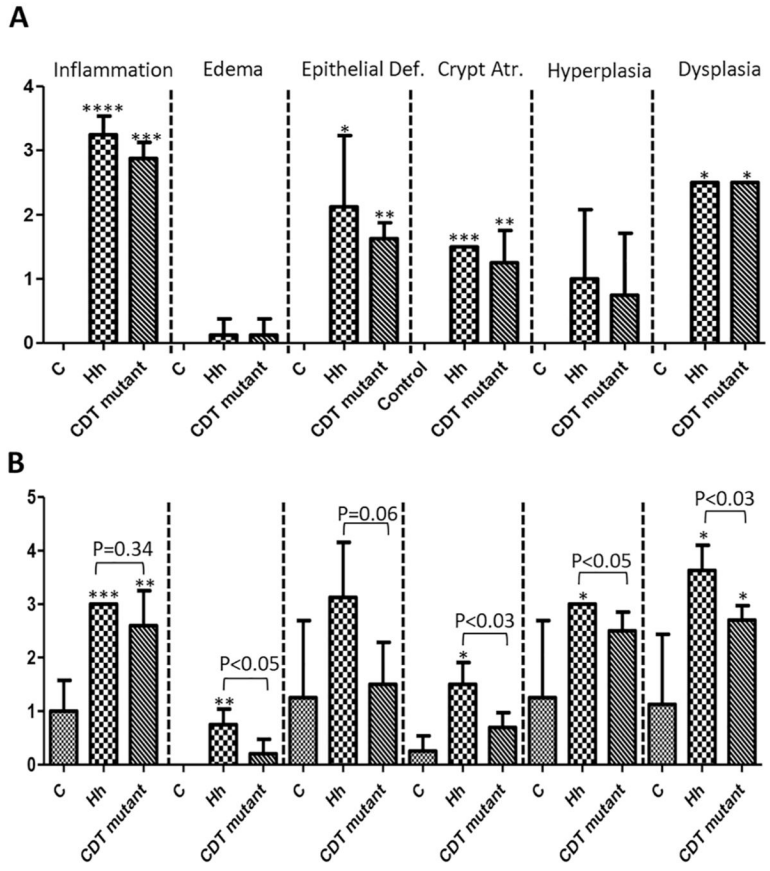

Figure 1.

Pathological scores of the individual lesions in the cecum and ileocecocolic junction (Cecum/ICC). (A) 10 WPI and (B) 20 WPI. The data are shown as means ± the standard deviations (n=3 to 5). At 10 WPI, Hh- or the HhCDT mutant-infected mice developed more severe inflammation, epithelial defects, crypt atrophy, dysplasia compared with uninfected controls, whereas there was no significant difference in the scores of all the categories between Hh- and HhCDT mutant-infected mice. At 20 WPI, Hh-infected mice developed more severe crypt atrophy, hyperplasia and dysplasia, but had similar degrees of inflammation compared with the HhCDT mutant-infected mice. There was no significant differences noted for some pathological lesions between the infected mice and the uninfected controls, which is due to spontaneous pathology developed in 2 controls. * represents P values when compared with the uninfected controls: * <0.05. **<0.01, ***<0.001, **** <0.0001.

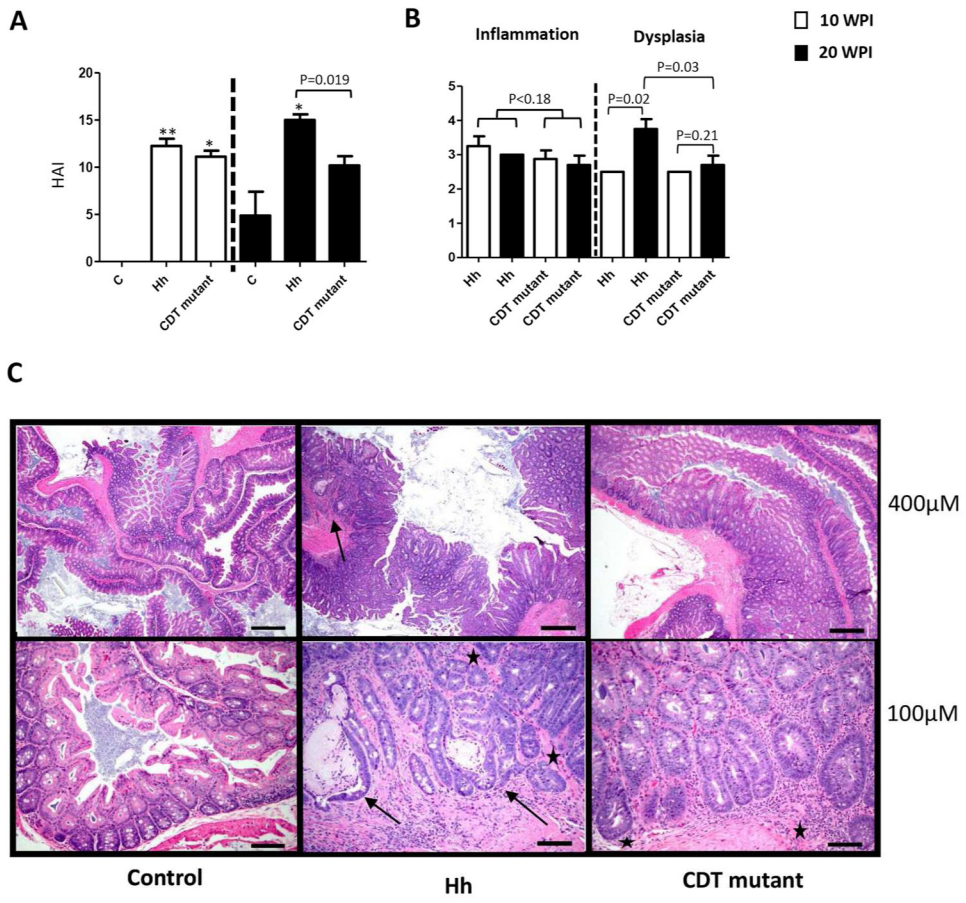

Figure 2.

Cecum/ICC pathology. (A) Histologic activity index (HAI) scores. Tissues from mice dosed with Hh, or the HhCDT mutant or vehicle alone were graded for inflammation, edema, epithelial defects, crypt atrophy, hyperplasia, and dysplasia. The ICC/Cecum HAI scores was generated by combining scores for all criteria. The HAI was comparable at 10 WPI, but was significantly higher at 20 WPI compared with the HhCDT mutant-infected mice. (B) 10 WPI (open bars) versus 20 WPI (solid bars) comparison for inflammation and preneoplastic dysplasia between Hh-infected mice and the HhCDT mutant-infected mic. From 10 WPI to 20 WPI, there were no significant differences in the inflammation grades between Hh- and the HhCDT mutant-infected mice, whereas Hh infection promoted progression of dysplasia to cancer. C) H&E panel showing representative low (top) and high (bottom) magnification images from Cecum/ICC of the different groups of mice at 20WPI. The uninfected control images (left top and bottom images) show lack of any significant inflammation or other associated morphological alterations. In the Hh infected animal (middle top and bottom panels), there is prominent diffuse inflammation, epithelial hyperplasia and high grade glandular dysplasia with focal submucosal invasion-carcinoma (arrows). Note cystically distended, horizontal spreading elongate invasive glands (arrows) surrounded by inflammatory cells embedded within the submucosa (middle bottom image). In the representative Cecum/ICCimages of the HhCDT mutant mice (right top and bottom images), there is slightly lesser degree of overall pathology with inflammation associated moderately

dysplastic glands but with no submucosal invasion. ★ Denotes the limit of muscularis mucosa. * represents P values when compared with the uninfected controls: ***<0.001, **** <0.0001.

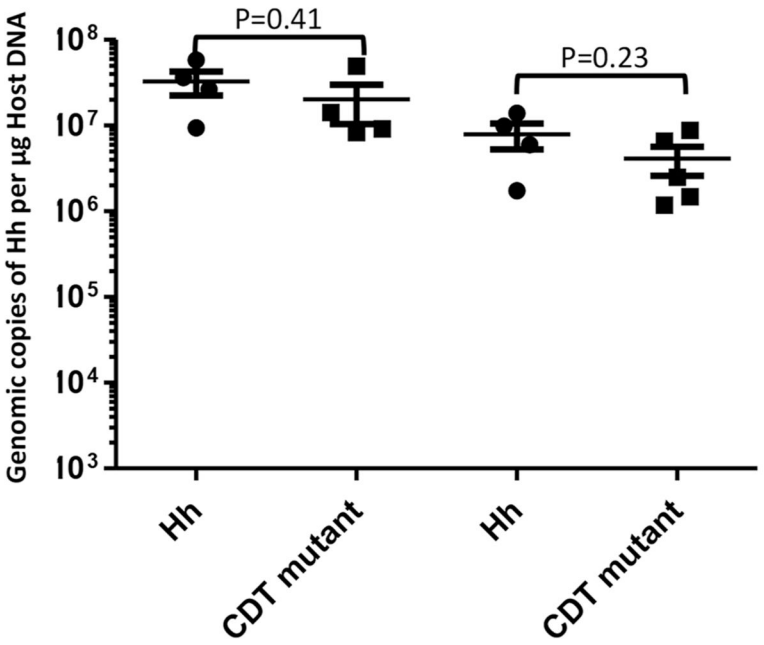

Figure 3.

HhCDT-deficiency did not affect the colonization levels of the HhCDT mutant compared with Hh. There were no significant differences in colonization levels between Hh and the HhCDT mutant at both time-points. The numbers on the y axis represent the copies of the Hh genome expressed per µg murine DNA in the samples.

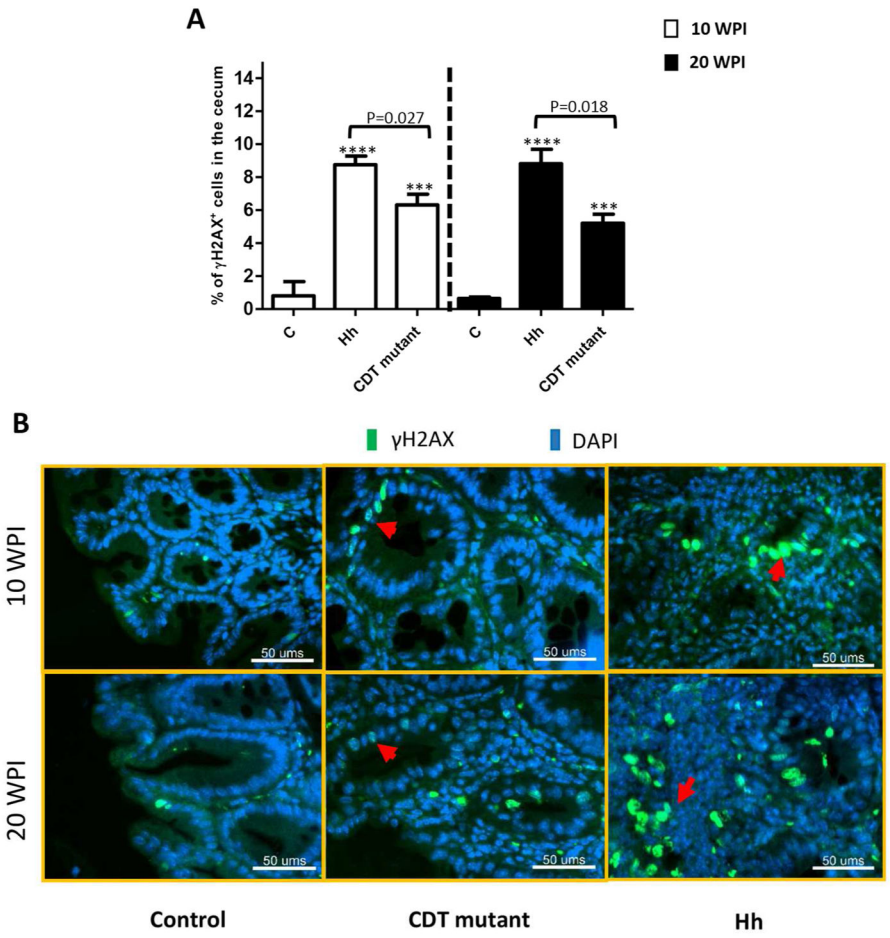

Figure 4.

γH2AX foci$^+$ epithelial cells in the ICC/Cecum. (A) The percentage of γH2AX foci$^+$ epithelial cells in the cecum/ICC tissues from mice dosed with Hh, or the HhCDT mutant or vehicle alone at both 10 and 20 WPI. Hh infection significantly elevated the percentage of γH2AX foci$^+$ epithelial cells compared with the HhCDT mutant infection. All the infected mice contained more γH2AX foci$^+$ epithelial cells than the uninfected controls. (B) The representative γH2AX staining of cecal epithelial cells. * represents P values when compared to the sham controls: ***<0.001, ****<0.0001.

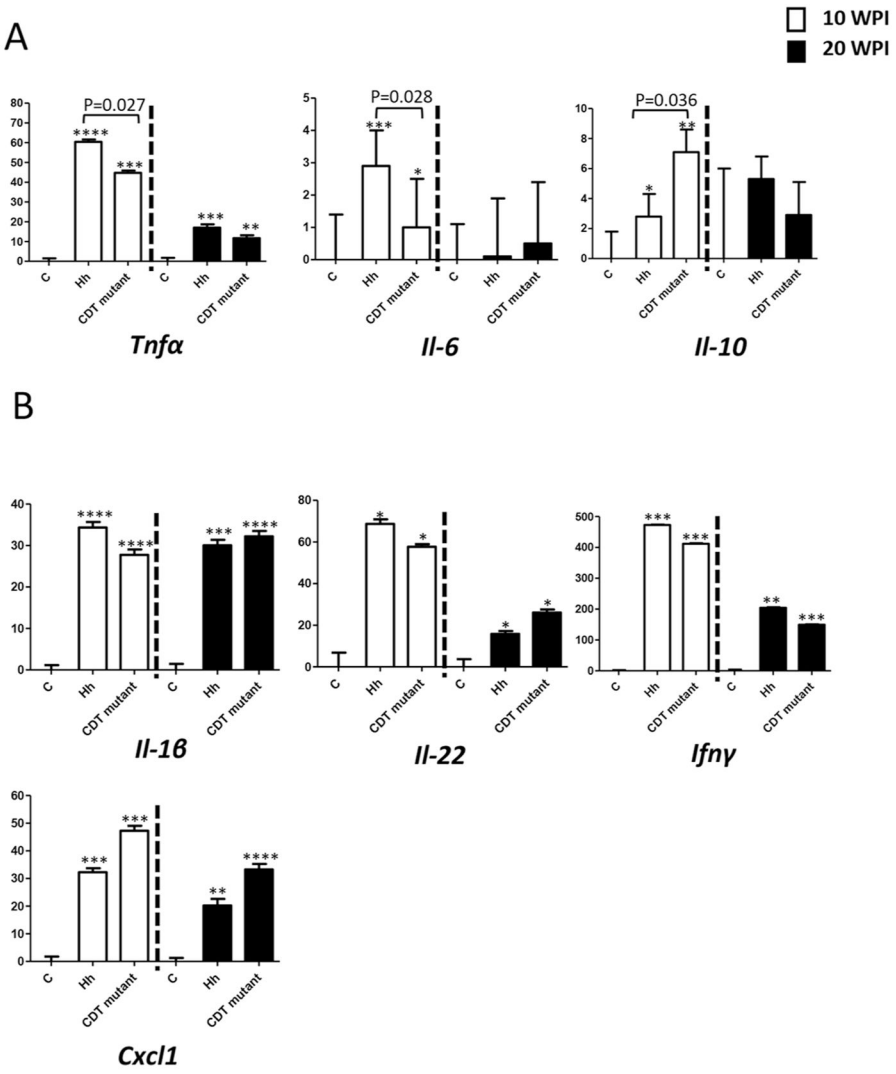

Figure 5.

Relative mRNA levels of select cecal genes contributing to inflammation and carcinogenesis. The significant transcriptional differences were found for some genes (A) and not for the others (B) between Hh- and the HhCDT-infected mice. For the comparison of mRNA, the target mRNA was normalized to that of the "house-keeping: gene *Gapdh*. Numbers on the y axis represent mean fold change of the individual mRNA levels in reference to the control group (defined as 0). Bars, standard deviations. * represents P values when compared to the sham controls: * <0.05, **<0.01, ***<0.001.

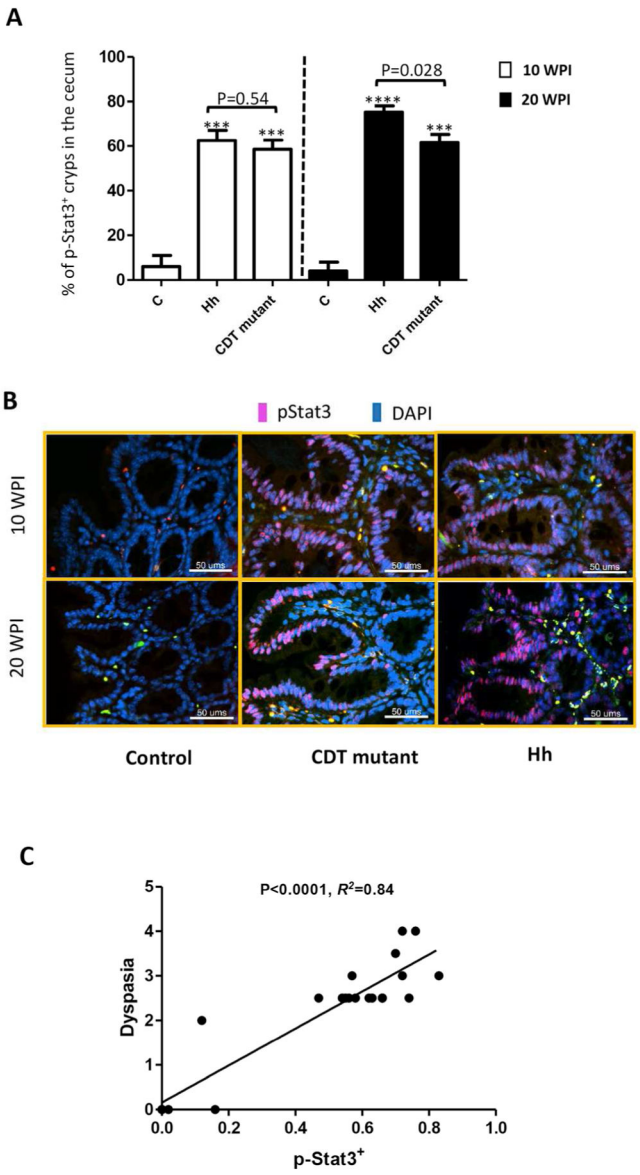

Figure 6.

HhCDT-deficiency decreased the potential of *H. hepaticus* to induce activation of Stat3 at 20 WPI. (A) The percentage of the phospho-Stat3 foci^{+} cells in the cecal tissues from mice dosed with Hh, or the HhCDT mutant or vehicle alone at both 10 and 20 WPI. Hh-infected mice contained significantly more phospho-Stat3 foci^{+} cells in the cecum compared with the HhCDT mutant-infected mice at 20 WPI, but at 10 WPI. (B) The representative phospho-Stat3 staining images of the ICC/cecal tissue. (C) Linear regression analysis showing that there is the positive correlation between the numbers of the phospho-Stat3 foci^{+} cells and the scores of dysplasia. * represents P values when compared to the sham controls: ***<0.001, ****<0.0001.